Journal of Orthopaedic Translation 47 (2024) 249–260

Contents lists available at ScienceDirect

Journal of Orthopaedic Translation

journal homepage: www.journals.elsevier.com/journal-of-orthopaedic-translation

Original Article

Localized delivery of metformin via 3D printed GelMA-Nanoclay hydrogel scaffold for enhanced treatment of diabetic bone defects

Hetong Li [*,1], Beini Mao [1], Jintao Zhong, Xiuwang Li, Hongxun Sang [**]

Department of Orthopedic Surgery, Shenzhen Hospital, Southern Medical University, Shenzhen, Guangdong, China

ARTICLE INFO

Keywords:
3D printing
Diabetic bone defects
Hydrogel scaffold
Immunomodulation
Metformin
Osteogenesis

ABSTRACT

Background: Diabetic bone defects present significant challenges for individuals with diabetes. While metformin has been explored for bone regeneration via local delivery, its application in treating diabetic bone defects remains under-explored. In this study, we aim to leverage 3D printing technology to fabricate a GelMA-Nanoclay hydrogel scaffold loaded with metformin specifically for this purpose. The objective is to assess whether the in situ release of metformin can effectively enhance osteogenesis, angiogenesis, and immunomodulation in the context of diabetic bone defects.

Materials and methods: Utilizing 3D printing technology, we constructed a GelMA-Nanoclay-Metformin hydrogel scaffold with optimal physical properties and biocompatibility. The osteogenic, angiogenic, and immunomodulatory characteristics of the hydrogel scaffold were thoroughly investigated through both in vitro and in vivo experiments.

Results: GelMA10%-Nanoclay8%-Metformin5mg/mL was selected as the bioink for 3D printing due to its favorable swelling rate, degradation rate, mechanical strength, and drug release rate. Through in vitro investigations, the hydrogel scaffold extract, enriched with metformin, demonstrated a substantial enhancement in the proliferation and migration of BMSCs within a high-glucose microenvironment. It effectively enhances osteogenesis, angiogenesis, and immunomodulation. In vivo experimental outcomes further underscored the efficacy of the metformin-loaded GelMA-Nanoclay hydrogel scaffold in promoting superior bone regeneration within diabetic bone defects.

Conclusions: In conclusion, while previous studies have explored local delivery of metformin for bone regeneration, our research is pioneering in its application to diabetic bone defects using a 3D printed GelMA-Nanoclay hydrogel scaffold. This localized delivery approach demonstrates significant potential for enhancing bone regeneration in diabetic patients, offering a novel approach for treating diabetic bone defects.

The translational potential of this article: Our study demonstrates, for the first time, the successful loading of the systemic antidiabetic drug metformin onto a hydrogel scaffold for localized delivery. This approach exhibits significant efficacy in mending diabetic bone defects, presenting a promising new avenue for the treatment of such conditions.

1. Introduction

Diabetes mellitus (DM) is a metabolic disease characterized by elevated blood sugar (hyperglycemia) and systemic chronic inflammation, which can lead to chronic damage to multiple organs and tissue [1]. In 2019, there were approximately 463 million patients worldwide. The number of people living with diabetes is expected to increase to 550 million by 2030 [2,3]. Diabetic bone defect is one of the serious complications faced by patients with diabetes. This special type of bone defect brings severe challenges to patients' quality of life and health status. Clinically, patients with DM have impaired bone repair and angiogenesis abilities after fractures, often leading to bone nonunion, delayed healing or bone defects, and there is still a lack of effective solutions [4]. Traditional treatment methods may be effective in

* Corresponding author. No.1333 Xinhu Street, Shenzhen, Guangdong, 518000, China.
** Corresponding author. No.1333 Xinhu Street, Shenzhen, Guangdong, 518000, China.
E-mail addresses: Heatonlee@outlook.com (H. Li), Maobeini187@163.com (B. Mao), 1243513@qq.com (J. Zhong), 120821223@qq.com (X. Li), Hxsang@smu.edu.cn (H. Sang).
[1] Hetong Li and Beini Mao contributed equally to this work.

https://doi.org/10.1016/j.jot.2024.06.013
Received 24 January 2024; Received in revised form 28 May 2024; Accepted 20 June 2024

alleviating general bone defects, but the treatment effect for diabetic bone defects is not ideal [5]. Therefore, there is an urgent need to develop an innovative therapeutic strategy to improve the therapeutic efficacy and enhance bone regeneration capacity in diabetic patients.

Metformin, an oral medication prescribed for type 2 diabetes, primarily stabilizes blood sugar levels by reducing hepatic glycogen production, enhancing insulin sensitivity, and slowing intestinal glucose absorption [6]. Beyond its systemic hypoglycemic effects, foundational research has revealed that in a high-glucose environment, metformin elevates ALP activity in MC3T3-E1 cells, fostering the formation of bone mineralized nodules. Moreover, it upregulates osteogenesis-related transcription factors, including runt-related transcription factor 2 (RUNX2), osteocalcin (OCN), and the expression of type I collagen (COL-I)-related genes [7]. Furthermore, metformin exhibits anti-inflammatory properties by inhibiting M1 polarization and the production of pro-inflammatory factors in synovial macrophages. This anti-inflammatory action plays a protective role against cartilage degeneration and synovitis [8]. Previous studies have also highlighted metformin's collaboration with mesenchymal cells, promoting Akt/mTOR activation and vascular endothelial growth factor (VEGF)-mediated angiogenesis during diabetic wound healing [9]. Collectively, metformin demonstrates osteogenic, anti-inflammatory, and angiogenic properties, making it pivotal in the reparative process of diabetic bone defects. While metformin has been explored for bone regeneration through local delivery, its use in treating diabetic bone defects by being loaded onto 3D-printed biomaterial scaffolds for in situ drug release remains to be studied [10,11].

To facilitate the stable and sustained release of metformin at the site of bone defects, we have introduced an innovative treatment approach. This involves utilizing a high-strength biodegradable hydrogel scaffold as a carrier for metformin delivery in the treatment of diabetic bone defects. The primary components of the hydrogel comprise gelatin methacrylate (GelMA) and Nanoclay. GelMA not only preserves the biocompatibility of gelatin but also readily undergoes cross-linking under light exposure due to the presence of photosensitizers [12]. However, the inherent challenges of GelMA, including low viscosity and an extended cross-linking time, make direct printing with extrusion-based 3D printing technology difficult. To address this, we redesigned the biomaterial ink for the GelMA scaffold, incorporating Nanoclay. This modification aims to strike a balance between printability and biocompatibility, leveraging Nanoclay's shear stress-dependent phase change properties that obviate the need for additional sol–gel processes. The gel transition conditions are highly conducive to extrusion-based 3D printing [13,14]. Furthermore, preceding studies have indicated that Nanoclay itself can release magnesium and silicon into the circulation, fostering the osteogenic differentiation of Bone Marrow Stromal Cells (BMSCs) [15]. This addition introduces an extra dimension to the hydrogel, contributing to its healing efficacy.

In this investigation, we formulated a range of GelMA-Nanoclay bioinks and leveraged 3D printing technology to construct metformin-loaded GelMA-Nanoclay hydrogel scaffolds. The sustained release of metformin from these scaffolds directly enhances the osteogenic and angiogenic capacities of the site of the defect. Simultaneously, it can inhibit the polarization of M1 macrophages and promote the polarization of M2 macrophages, thereby reducing inflammation. This triple regulatory effect of the hydrogel scaffold underscores its potential. Consequently, our approach introduces a promising metformin-loaded, high-strength, biodegradable hydrogel scaffold with triple-regulated functions—osteogenic, angiogenic, and immunomodulatory. This innovative strategy aims to orchestrate efficient bone regeneration within the complex diabetic microenvironment.

2. Materials and methods

2.1. Preparation of hydrogels

GelMA-nanoclay copolymer hydrogels were prepared by photo-initiated radical copolymerization. Briefly, an appropriate amount of GelMA and Nanoclay were dissolved in a solution containing 0.1 wt% photoinitiator (Lithium Phenyl (2,4,6-trimethylbenzoyl) phosphinate, LAP) according to the designed formula. A series of hydrogels were prepared with GelMA (10 %) and varying initial Nanoclay (0 %, 4 %, 8 %, 12 %) monomer concentrations in this study. To simplify the discussion, the obtained hydrogels were coded as GelMA-NanoclayX, where X represents the initial mass percentage concentration of nanoclay.

2.2. Dynamic swelling test of hydrogels

GelMA-NanoclayX hydrogels with varied initial monomer concentrations of nanoclay were prepared in the form of cylinders with a diameter of 5 mm and a height of 5 mm. The swelling ratio of the hydrogels was calculated using the equation: SR = Wt/Wi, where Wt is the wet weight of the swollen hydrogels at time t (t is the time the hydrogel was immersed in deionized water), and Wi is the initial wet weight of the hydrogels. All experiments were performed in triplicate. The EWCs of the hydrogels were determined as described in the reported method [16].

2.3. Degradation test of hydrogels

Circular samples with a 5 mm diameter and 5 mm thickness were incubated in deionized water at 37 °C in a reciprocal shaking incubator at 60 rpm. The solution was renewed every three days. At predetermined time intervals, the hydrogels were removed from the solution, freeze-dried, and weighed. The percent remaining mass was calculated using the equation: $D\% = (W_{o,dry} - W_{t,dry})/W_{o,dry} \times 100\ \%$, where $W_{o,dry}$ is the initial dry weight of the sample, and $W_{t,dry}$ is the dry weight at each incubated time point.

2.4. Mechanical properties of hydrogels

Mechanical tests were performed at room temperature after an equilibrium swelling state was achieved in deionized water using a Z050 universal biomechanical testing machine (ZwickRoell Group Inc., Germany). Cylindrical samples (diameter 5 mm, height 5 mm) were used for compression tests. The crosshead speed was set at 10 mm/min. At least eight samples were used in each mechanical test.

2.5. Drug release analysis

We first prepared a series of GelMA-Nanoclay solutions loaded with different metformin concentrations (2 mg/mL, 5 mg/mL, and 10 mg/mL), and the hydrogels were formed by UV light-initiated polymerization. The metformin release from GelMA-Nanoclay-Metformin hydrogels was characterized as follows. The hydrogels were immersed in 3 mL deionized water and shaken at 60 rpm at 37 °C. At different immersion time points, 500 μL solution was taken out and replaced with 500 μL fresh deionized water. The collected solution was appropriately diluted, and the maximum absorbance value at 233 nm was measured using UV spectrophotometry to calculate the mean drug release concentration. According to preliminary experimental results, the lowest detectable concentration of metformin is 0.208 μg/mL. Subsequently, we cultured rat BMSCs in three mean drug release concentrations (1, 2, and 3 μg/mL), and performed cell viability assays at 1, 4, and 7 days. To assess the impact of glucose on BMSCs viability, cells were cultured in minimum eagle medium (MEM) with varying glucose concentrations (5.6 mM, 11.1 mM, 16.7 mM, 25.0 mM, and 33.3 mM) for 1, 3, and 5 days. A cell

counting kit-8 (CCK-8, Beyotime, China) was used to evaluate the effect of different glucose concentrations on cell proliferation. After 72 h of culture in normal or high-sugar medium, the mRNA expression of OCN, VEGF, and TNF-α in these BMSCs was examined to determine the optimal dosage of metformin.

2.6. 3D printing of GelMA-Nanoclay hydrogel scaffolds

3D printed hydrogel scaffolds were produced using a Bio 3D printer (BioX, Cellink, Sweden). Briefly, the pre-hydrogel (GelMA10%-Nanoclay8%-Metformin5 mg/mL) strands were plotted onto a glass slide through a conical needle with an inside diameter of 250 μm (100 kPa, 2 mm/s, 25 °C). Each layer adhered to the underlying layer perpendicularly to form a 0°/90° structure, and the spacing between each strand was set at 750 μm. Sixteen layers of GelMA-Nanoclay-Metformin hydrogel scaffolds were fabricated after post-crosslinking with UV light irradiation. Initially, a rectangular hydrogel scaffold measuring 10 mm*10 mm*4 mm was constructed. Following the completion of the disinfection and sterilization process, a cylindrical structure with a diameter of 4 mm and a height of 4 mm was extracted from the aforementioned cube for in vivo bone defect repair.

2.7. Scanning electron microscopy (SEM) analysis and energy-dispersive X-ray spectroscopy (EDS) analysis

To assess the microstructure of 3D printed hydrogel scaffolds, the samples were gold-palladium coated and then observed under a scanning electron microscope (Hitachi Model TM-1010, Japan). Meanwhile, EDS analysis was performed using an Oxford X-MAX 80 system to determine the presence of magnesium, silicon, and nitrogen elements of the GelMA-Nanoclay-Metformin hydrogel scaffolds.

2.8. In vitro biological functional analysis of hydrogel scaffolds

2.8.1. Isolation and characterization of rat BMSCs

Rat BMSCs were isolated from the femurs and tibias of Sprague–Dawley (SD) rats, following a standardized protocol. To characterize the isolated BMSCs, flow cytometry was performed to assess the expression of surface markers CD45, CD73, and CD90. The differentiation potential of the BMSCs was assessed by inducing differentiation into osteogenic, adipogenic, and chondrogenic lineages using specific induction media.

2.8.2. Osteogenic activity analysis

To evaluate the osteogenic capacity, BMSCs and hydrogel extracts were incubated in normal (5.6 mM) or high glucose medium (33.3 mM) for 7 days and then stained for alkaline phosphatase (ALP). In addition, after 21 days of culture, calcium nodules were verified using Alizarin Red S (ARS) staining kit (Cyagen, Guangzhou, China). Image Pro Plus 6.0 software was used to quantitatively analyze the staining intensity of ALP and alizarin red. For details see supplementary materials.

2.8.3. Angiogenic activity analysis

BMSCs and hydrogel extracts were cultured in either normal or high glucose medium. The expression of vascular endothelial growth factor (VEGF) was assessed after 72 h. Gene expression analysis was performed using quantitative real-time polymerase chain reaction (qRT-PCR) with the ABI 7500 RT-PCR System (Applied Biosystems, MA, USA) and SYBR Green PCR Master Mix (Toyobo Life Science, Osaka, Japan). Additionally, we measured the expression levels of bone-related markers, including osteocalcin (OCN) and receptor activator of nuclear factor kappa-B ligand (RANKL), as well as the inflammation-related gene tumor necrosis factor-alpha (TNF-α).

2.8.4. Immunomodulatory effects analysis

RAW264.7 cells were seeded in 6-well plates at a density of 4×10^5 cells per well and allowed to adhere overnight. To induce M1 polarization, cells were treated with 100 ng/mL lipopolysaccharide (LPS) and 20 ng/mL interferon-gamma (IFN-γ) for 72 h. For M2 polarization, cells were treated with 20 ng/mL interleukin-4 (IL-4) and 20 ng/mL interleukin-13 (IL-13) for 72 h. During polarization, cells were simultaneously treated with extracts from different hydrogel scaffolds. After polarization, cells were harvested, stained with PE-conjugated anti-CD86 and FITC-conjugated anti-CD206 antibodies, and analyzed using a BD FACSCalibur flow cytometer. Data were analyzed to assess the effects of different hydrogel scaffolds on M1 and M2 macrophage polarization by comparing the expression levels of CD86 and CD206.

2.8.5. Cell proliferation analysis

BMSCs at a density of 4×10^5 cells/mL were co-cultured with 3D-printed hydrogel scaffold extracts in normal or high glucose medium to evaluate its cytotoxicity and viability. A CCK-8 was used to evaluate the effect of 3D-printed hydrogel scaffold extracts on cell proliferation at 1, 3, and 5 days, respectively. The cytotoxicity was assessed by a live-dead staining kit (CFSE, Dojindo Laboratories, Japan) at 72 h according to the manufacturer's guidelines. After the live-dead staining, the cells were imaged with a fluorescence microscope (X71, Olympus), and cell viability was calculated using ImageJ software. For details, see supplementary materials.

2.9. Wound healing assay

Wound healing is a method to evaluate cell migration ability. In brief, BMSCs (4×10^5 cells per well) were seeded into a 6-well plate and incubated at 37 °C under 5 % CO2. After the cells were 90 % confluent, a 200-μL pipette tip was used to create a scratch in the cell layer. Following three washes with aseptic PBS to remove cell debris, the medium was replaced with 0.5 % serum containing GelMA 10%-Nanoclay 8 % or GelMA 10%-Nanoclay 8%-Metformin5 mg/mL hydrogel extracts. At 0 and 12 h, images were captured using an inverted microscope. Corresponding data (i.e., migration areas) were calculated using ImageJ.

2.10. In vivo biological functional analysis of hydrogel scaffolds

2.10.1. Animal models

The animal protocol was approved by the Animal Ethics Committee of the Southern Medical University Shenzhen Hospital. A high-fat diet (HFD)/streptozotocin (STZ) (Sigma Aldrich)-induced diabetes model was established as described in a previous study [17]. A total of 60 SD rats were utilized to establish a critical-size bone defect model in the femoral condyle on one side, with a cylindrical bone defect of 4 mm diameter and 4 mm depth created vertically from the lateral condyle of the rat femur. Normal rats (n = 12) were used as a control group (Control). Diabetic rats were divided into four groups (n = 12 in each group), namely, untreated bone defect group (DM), autologous bone transplantation group (DM + AB), GelMA-Nanoclay hydrogel scaffold group (DM + S), metformin-loaded GelMA-Nanoclay hydrogel scaffold group (DM + MetS). For details, see supplementary materials.

2.10.2. Micro computed tomography (Micro-CT) analysis

Four and eight weeks after surgery, the rats (n = 6 in each group) were euthanized, and the femurs were explanted and fixed in 4 % (w/v) buffered paraformaldehyde. The newly formed bone in the bone defect was assessed using a micro-CT system (SkyScan 1172, Bruker, Belgium). The scanner was set at a voltage of 70 kV, a current of 110 mA, and a resolution of 12 μm/pixel. The region of interest (ROI) was defined as a pre-established bone defect measuring 4 mm in diameter and 4 mm in depth in the rat femoral condyle. The bone mineral density (BMD), ratio of bone volume to tissue volume (BV/TV), trabecular number (Tb.N) and trabecular number thickness (Tb.Th) were quantitatively determined.

2.11. Histological staining

After the micro-CT analysis, the samples were decalcified in 15 % (w/v) ethylenediaminetetraacetic acid (EDTA), dehydrated through a series of ethanol, embedded in paraffin, and longitudinally sectioned into slices with an approximate thickness of 5 μm using a paraffin microtome (Leica EG 1160). Routine H&E and Masson staining were used to observe the morphological changes in the specimens under an optical microscope, and bone histomorphometry was employed to quantitatively assess the area of newly formed bone.

2.12. Immunohistochemical (IHC) staining

IHC staining was used to identify the levels of Col-I, OCN, receptor activator of nuclear factor kappa-B ligand (RANKL), inducible nitric oxide synthase (iNOS), arginase-1 (Arg-1), CD68, CD206, and VEGF markers. For details, see supplementary materials.

2.13. Data analysis and statistics

Data are expressed as mean ± standard deviation (SD). All the experiments were analyzed by one-way analysis of variance (ANOVA) with Tukey' post hoc test. For all testing, the level of significance was set at $*p < 0.05$ and $**p < 0.01$.

3. Results

3.1. Characterization of GelMA-Nanoclay hydrogels

3.1.1. Dynamic swelling test

With an increase of NanoClay content at fixed GelMA concentration, the swelling ratio and the time to reach a swelling equilibrium of the GelMA-NanoClay hydrogels decrease by a different extent. The equilibrium swelling ratio of GelMa-NanoClay hydrogels is 0%NanoClay (2.75), 4%NanoClay (2.45), 8%NanoClay (1.85), and 12%NanoClay (1.60) (Fig. 1A).

3.1.2. Degradation test

As shown in Fig. 1B, the degradation time of GelMA-NanoClay hydrogels at 4 concentrations ranged from 6 to 70 days. With an increment of NanoClay at a fixed GelMA content, the degradation rate is decreased significantly.

3.2. Mechanical properties

Fig. 1C, D presents the compressive stress–strain curves of the GelMA-NanoClay hydrogels at different concentrations. The mechanical strengths are considerably increased with the increment in content of NanoClay. It is noted that the GelMA-NanoClay8% and GelMA-NanoClay12 % hydrogels all demonstrate excellent mechanical properties

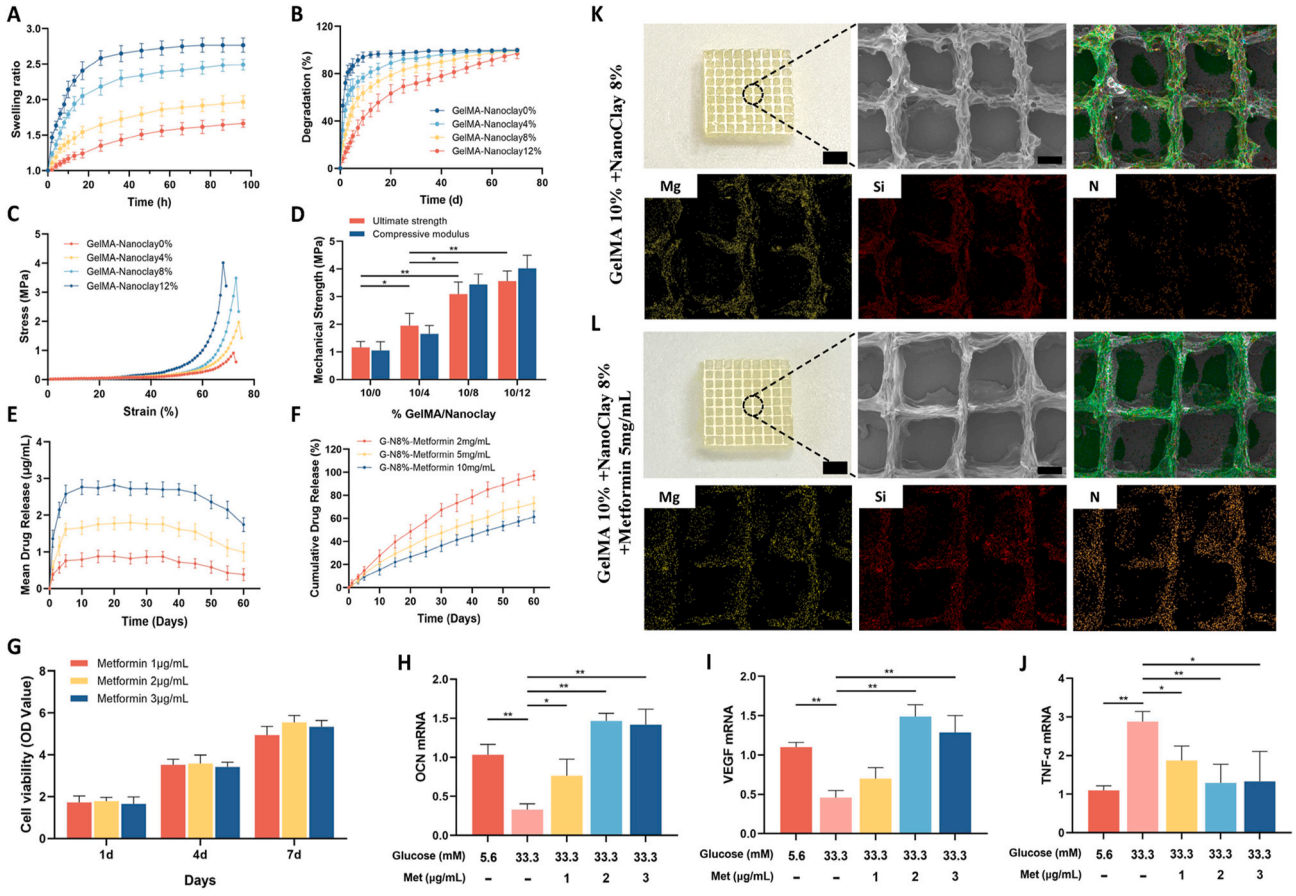

Fig. 1. A) Dynamic swelling behaviors and B) In vitro degradation behaviors of GelMA-NanoclayX hydrogels in deionized water. C) Compressive stress–strain curves of the GelMA-NanoclayX hydrogels. D) The effect of the bioink concentration on the mechanical strength. E-F) In vitro metformin release profile from metformin-loaded GelMA-Nanoclay8% as a function of time. G) Proliferation of BMSCs in culture medium with different metformin concentrations (1 μg/mL, 2 μg/mL and 3 μg/mL) on days 1, 4, and 7. H-J) Expression of OCN, VEGF, and TNF-α mRNA in BMSCs in normal or high-glucose medium after 72 h. K-L) The schematic diagram and scanning electron microscopy (SEM) images of the 3D-printed hydrogel scaffolds, along with the energy dispersive spectroscopy (EDS) analysis. (scale bar: thick bar = 2.5 mm, thin bar = 250 μm). (Statistical analysis of the hydrogel ultimate strength data was conducted, and all the results are presented as means ± SD, $*p < 0.05$, $**p < 0.01$).

with robust ultimate strength (3.1 and 3.6 MPa), and compressive modulus (3.3 and 4.1 MPa).

3.2.1. Drug release analysis

After thoroughly evaluating the swelling, degradation, and mechanical property data, and conducting preliminary experiments to assess the printability of different bioink concentrations, we ultimately opted for the GelMA-NanoClay 8 % concentration bioink for further investigation. The in vitro release profiles of three concentrations of metformin (2, 5 and 10 mg/mL) were studied. As shown in Fig. 2E and F, the amounts of metformin that were released increased at a relative rapid rate during the first 5 days and remained fairly steady for 2 months. Among them, the GelMA-NanoClay hydrogel loaded with 5 mg/mL metformin can sustain a release of approximately 1.8 μg/mL, which is similar to the blood drug concentration of 2 μg/mL after oral administration of metformin in humans (Fig. 1E and F) [18]. CCK8 results demonstrate that metformin concentrations of 1–3 μg/mL do not exert harmful effects on the proliferation of BMSCs (Fig. 1G), while a significant decrease in the proliferation capacity of BMSCs was observed when the glucose concentration reached 33.3 mM. Therefore, the normal medium used in this experiment had a glucose concentration of 5.6 mM, whereas the high-glucose medium had a concentration of 33.3 mM (Supplementary Fig. 1). After 72 h of culture in normal or high-glucose medium, the addition of 2 μg/mL and 3 μg/mL of metformin showed a significant impact on the mRNA expression of OCN, VEGF, and TNF-α in BMSCs (Fig. 1H–J). We prefer to choose the lowest drug dose, which is 2 μg/mL of metformin, for subsequent experiments. Therefore, our following experiments will utilize GelMA-NanoClay 8 % hydrogel loaded with 5 mg/mL of metformin for 3D printing of the scaffold.

3.3. 3D printing and SEM&EDS analysis of hydrogel scaffolds

The schematic and SEM morphology of the 3D-printed hydrogel scaffolds (both unloaded and metformin-loaded) are shown in Fig. 1K and L. The interconnected microscopic pores are orderly arranged and uniform. EDS analysis results indicate that the GelMA-NanoClay scaffolds contain evenly distributed magnesium and silicon elements, which are essential components of NanoClay. After the addition of metformin, abundant nitrogen elements were detected, suggesting that metformin is uniformly distributed within the 3D-printed scaffolds.

3.4. In vitro biological functional analysis of hydrogel scaffolds

3.4.1. Characterization of BMSCs

We successfully induced the differentiation of the isolated BMSCs into osteogenic, adipogenic, and chondrogenic lineages. Representative images of these differentiations are shown in Fig. 2A. Flow cytometry analysis was subsequently performed to characterize the surface marker expression of the isolated cells. The results demonstrated that the cells were negative for the hematopoietic marker CD45 and positive for the mesenchymal stem cell markers CD73 and CD90 (Fig. 2B). These findings confirm that the isolated cells were indeed BMSCs.

3.4.2. Osteogenic activity analysis

In a high-glucose environment, extracts from both the GelMA-NanoClay-Metformin hydrogel scaffold induced heightened ALP activity and increased calcium nodule density in BMSCs. Semi-quantitative analysis showed that compared with the HG group, the ALP + area and Alizarin red + area only in the HG + MetS group were significantly increased (Fig. 2C). Bone-related markers expression levels at 72 h were further analyzed by qRT-PCR (Fig. 2D). High-glucose environment significantly reduced the expression of OCN gene in BMSCs, but significantly enhanced the expression of RANKL gene. OCN expression was significantly up-regulated in the HG + MetS hydrogel scaffold group. RANKL gene expression was significantly decreased compared with the HG and HG + S groups.

3.4.3. Angiogenic activity analysis

The VEGF expression in the HG group and the HG + S group was significantly lower than that in the N group. However, after loading metformin into the GelMA-NanoClay hydrogel, the VEGF expression in the HG + MetS group was significantly higher than that in both the HG group and the HG + S group (Fig. 2D). This indicates that in a high glucose environment, the metformin-loaded hydrogel scaffold exhibits a significant angiogenic capacity.

3.4.4. Immunomodulatory effects analysis

To clearly demonstrate the effects of the metformin-loaded hydrogel scaffold on macrophage phenotype and inflammatory status, we performed analyses using flow cytometry and qRT-PCR. Flow cytometry results indicated that we successfully induced the differentiation of RAW264.7 cells (M0) into M1 and M2 macrophages. During the differentiation process, we added extracts from hydrogel scaffolds, both with and without metformin, into the culture medium. The results showed that in the MetS group, CD86 expression was significantly reduced while CD206 expression was significantly increased compared to the control and S groups (Fig. 2E and F). This indicates that the metformin-loaded hydrogel scaffold can significantly inhibit M1 macrophage polarization while promoting M2 macrophage polarization. qRT-PCR results further demonstrated that a high glucose environment significantly increased the expression of TNF-α mRNA in BMSCs. In contrast, the HG + MetS group exhibited a significant reduction in TNF-α mRNA expression levels (Fig. 2D). These findings suggest that the metformin-loaded hydrogel scaffold has anti-inflammatory properties and the ability to modulate macrophage differentiation.

3.4.5. Cell proliferation analysis

In normal medium, the cell activity of the N + MetS group was no different from that of the N group, indicating that the metformin hydrogel scaffold had no cytotoxicity. In high-glucose medium, cell viability in the HG and HG + S groups was significantly reduced, and metformin-loaded hydrogel scaffolds could significantly improve the cell viability of BMSCs in high-glucose environment (Fig. 3A). The proliferation assessment of BMSCs using CCK-8 on days 1, 3 and 5 showed similar results. After culturing BMSCs in high-glucose medium for five days, the OD values of the HG group and HG + S group were significantly lower than those of the N group. The OD values of the HG + MetS group were significantly higher than those of the HG group and HG + S group (Fig. 3D).

3.5. Wound healing assay

Semi-quantitative analysis revealed that within a high glucose environment, the wound closure area of the HG + MetS group at 12 h was significantly smaller compared to both the HG and HG + S groups. This indicates that the metformin-loaded hydrogel scaffold exerts a more pronounced promotion effect on BMSC migration (Fig. 3B and C). These results indicate that the migration ability of BMSCs is inhibited in a high-glucose microenvironment, and the presence of metformin can rescue this situation.

3.6. In vivo biological functional analysis of hydrogel scaffolds

3.6.1. Micro-CT analysis

The GelMA-NanoClay-Metformin hydrogel scaffolds demonstrated the most favorable bone reconstruction through 8 weeks according to micro-CT. As shown in Fig. 4A, micro-CT analysis carried out at the end of 4 and 8 weeks after surgery presented vivid details of trabecular bone with 3D reconstruction. It was obvious that bone volume was increased in each group as time went by, while DM + MetS group induced bone regeneration best in bone defect compared to others. Such advantages

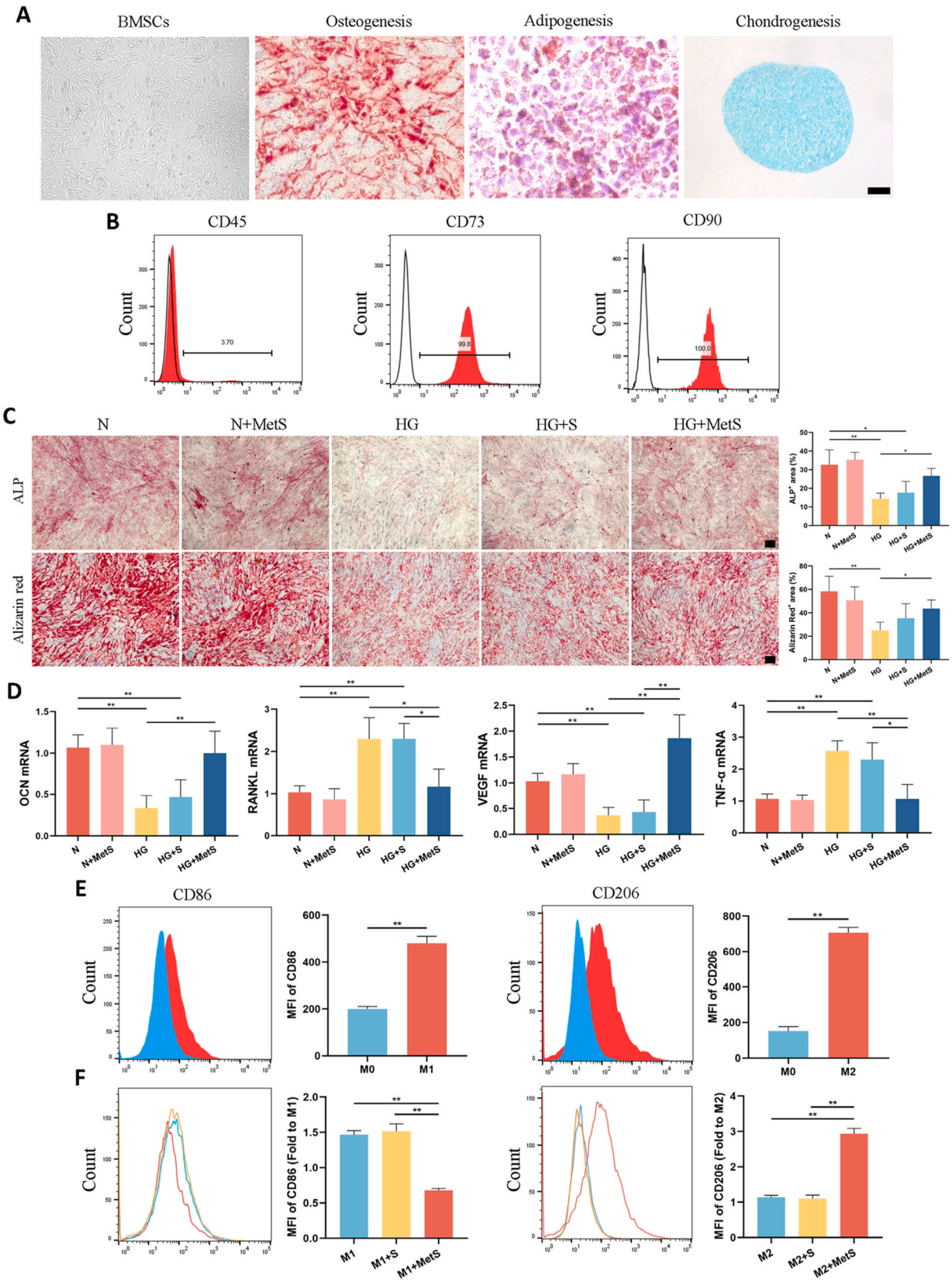

Fig. 2. A) The osteogenic, adipogenic, and chondrogenic differentiation potentials of BMSCs. B) Flow cytometry analysis of BMSCs surface markers CD45, CD73, and CD90. C) The expression of ALP after 7 days of incubation and calcium nodules after 21 days of incubation. D) mRNA expression levels of OCN, RANKL, VEGF, and TNF-α in BMSCs after 72 h of culture with different scaffold extracts. E) Representative graphs and statistical histograms comparing CD86 marker in the M1 induction group and CD206 marker in the M2 induction group to the M0 group. F) Representative graphs and quantitative analysis showing the effects of hydrogel scaffold extracts on CD86 (M1 marker) and CD206 (M2 marker). (scale bar: 250 μm). (N: Normal medium, HG: High glucose medium, MetS: Metformin scaffolds. Data are provided as means ± SD, $*p < 0.05$, $**p < 0.01$).

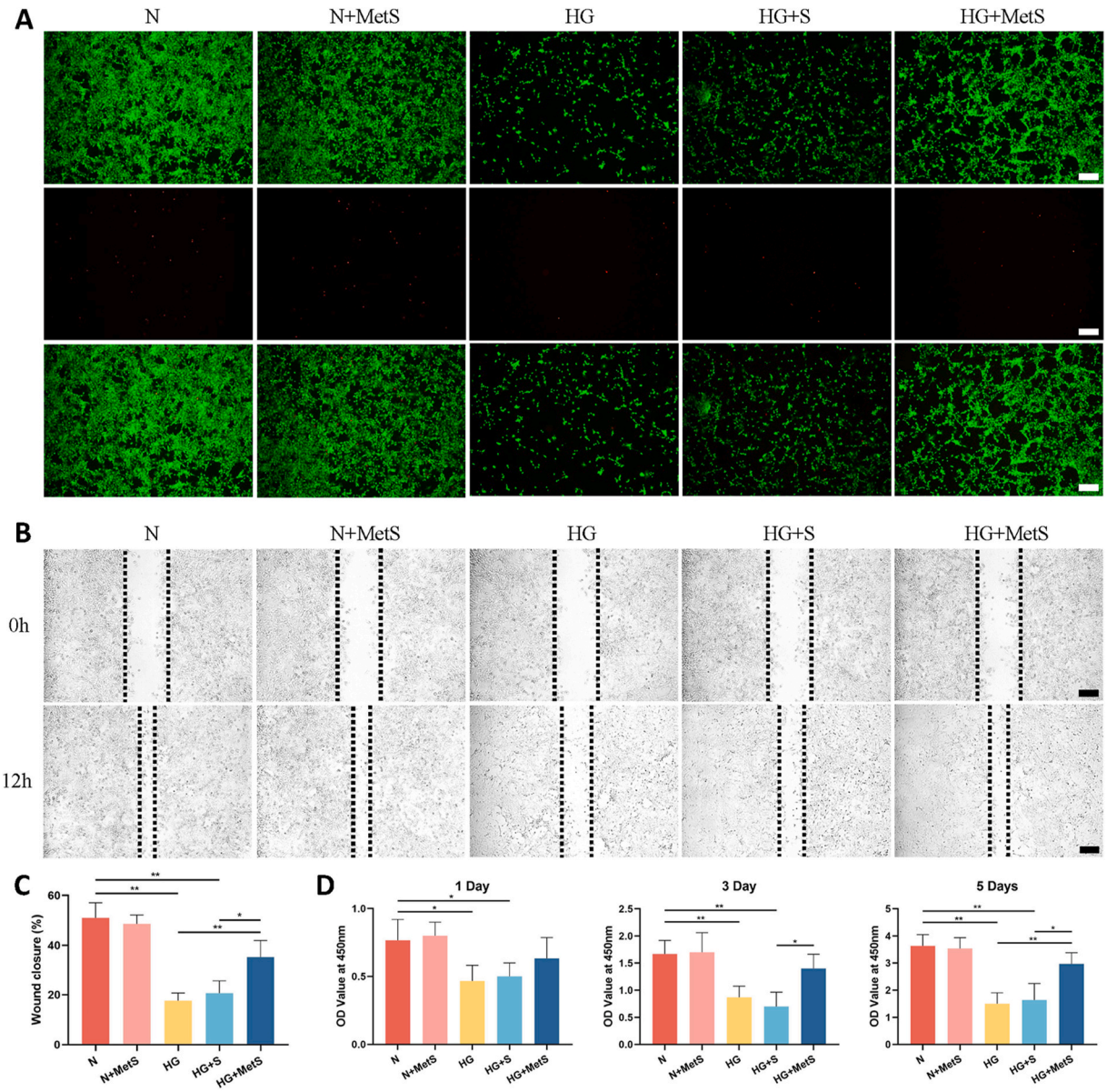

Fig. 3. The A) proliferation and B) migration of BMSCs comparison between scaffolds printed using GelMA-Nanoclay and GelMa-Nanoclay-Metformin hydrogels. (C) Quantitative analysis of BMSCs migration. D) Proliferation of BMSCs using GelMA-Nanoclay and Gelma-Nanoclay-Metformin hydrogel scaffold extracts in normal or high glucose medium on days 1, 3 and 5 (scale bar: 100 μm). (N: Normal medium. HG: High glucose medium. MetS: Metformin scaffolds. Data are provided as means ± SD, $^{*}p < 0.05$, $^{**}p < 0.01$).

were proved by quantification of BMD, BV/TV and Tb.N (Fig. 4B). Interestingly, the BMD of rat in the DM + AB group with autologous bone transplantation was also significantly higher than that in the DM group.

3.6.2. Histological analysis

From H&E staining at 4 weeks, almost no osteogenesis was seen in the bone defects of rats in the DM group and DM + S group, but bone remodeling was relatively active in the DM + MetS group. Because of the presence of autologous bone, obvious trabecular bone structure was observed in the bone defect in the DM + AB group (Fig. 5A). Masson staining had similar results (Fig. 5B). However, at 8 weeks, cortical and cancellous bone structure was gradually remodeled in Control and DM + MetS groups, but still few was seen in DM and DM + S, indicating poor bone repair, which was demonstrated by quantification of bone histomorphometry (Fig. 5C and D). In addition, Masson staining showed that autologous bone grafts also exhibited osteogenic capacity under diabetic conditions, but a disordered trabecular bone structure was observed, it shows that bone formation and bone resorption are locally imbalanced. The blood glucose levels of the rats were continuously detected after STZ injection. The results showed that the random blood glucose levels in all DM group were consistently above 16.7 mmol/L, indicating that all rats in these groups maintained a diabetic state (Fig. 5E).

3.6.3. Immunohistochemical analysis

As is shown in Fig. 6, diabetes leads to a decrease in OCN content and a significant increase in RANKL expression, reflecting the more active osteoclast production in a high-glucose microenvironment. Regardless of whether metformin is loaded, the GelMA-NanoClay hydrogel scaffold can significantly increase the expression of OCN, and it has been observed that when diabetic rats were subjected to autologous bone transplantation, the expression levels of OCN and RANKL were significantly increased, suggesting that in the pathological state of diabetes, autologous bone may cause excessive bone remodeling due to its

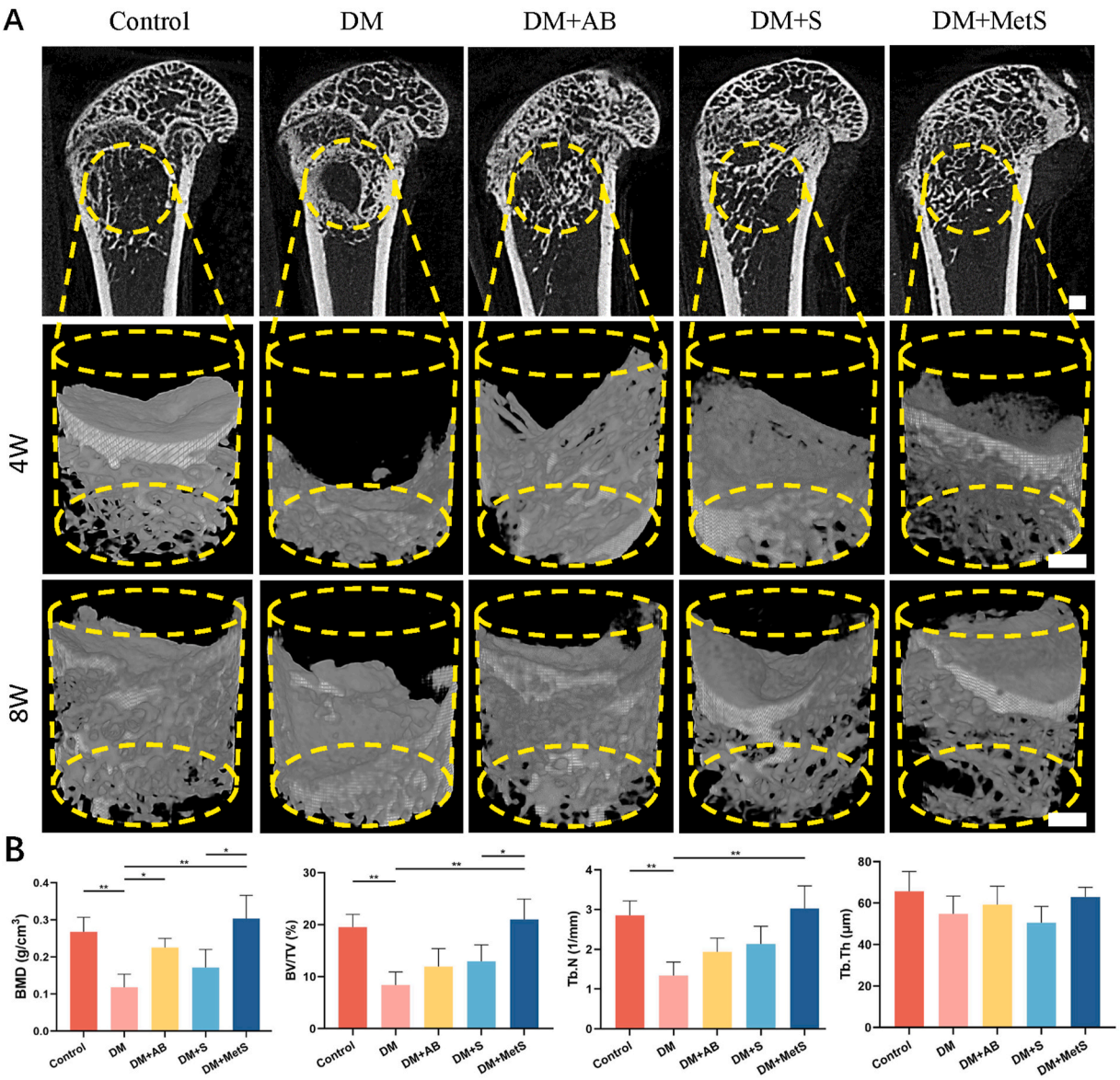

Fig. 4. A) Sagittal plane at 4 weeks and typical pictures of micro-CT of femurs of rats with bone defects at 4 and 8 weeks (scale bar: 1 mm, yellow circles represented the initial position of bone defect). B) Morphological parameters of the bone mineral density (BMD), bone volume/tissue volume (BV/TV), trabecular number (Tb.N), trabecular thickness (Tb.Th). (DM: diabetes mellitus, AB: autologous bone, MetS: Metformin scaffolds; n = 6 per group, data are provided as means ± SD, $*p < 0.05$, $**p < 0.01$). (For interpretation of the references to color in this figure legend, the reader is referred to the Web version of this article.)

inherent tissue activity. After metformin loading, the expression of OCN and RANKL in the DM + MetS group returned to normal levels, with no statistical difference from the Control group. Diabetes caused a significant increase in iNOS (inflammatory M1 marker) and CD68 (General macrophage marker) expression in bone defect areas. In situ metformin release of DM + MetS group led to a much fewer number of iNOS-positive and CD68-positive cells than DM, DM + AB, and DM + S groups, as well as a significant increase in Arg-1 and CD206 expression (anti-inflammatory M2 marker), which indicated that the metformin-loaded hydrogel scaffold has an anti-inflammatory effect and ability to regulate macrophage differentiation. In addition, compared with the contorl group, the expression of VEGF in the DM group was significantly reduced, and the VEGF content in the DM + MetS group was significantly higher than the DM, DM + AB and DM + S groups.

4. Discussion

Diabetes impairs bone regeneration primarily by inducing chronic low-grade inflammation due to hyperglycemia. This environment increases reactive oxygen species (ROS) production, leading to mitochondrial dysfunction in macrophages and promoting the secretion of inflammatory factors such as TNF-α, IL-6, and IL-1β. Additionally, the abnormal activation of the NF-κB signaling pathway in diabetes disrupts the immunoregulatory function of BMSCs, further exacerbating local inflammation and hindering bone repair [19]. As a result, diabetic bone defects pose a significant challenge for individuals with diabetes, as prolonged exposure to this condition disrupts bone metabolism, compromising bone quality and impeding regeneration [20,21]. To surmount the limitations of conventional treatments, our study introduces an innovative approach. Leveraging 3D printing technology, we precisely and controllably load metformin—an extensively used drug for systemic hypoglycemic control—into a hydrogel scaffold for in-situ release. This localized and targeted release mechanism enhances treatment efficiency, directly addressing the area of diabetic bone defect, thereby improving treatment specificity and efficacy. The hydrogel's primary components, GelMA and Nanoclay, are well-established

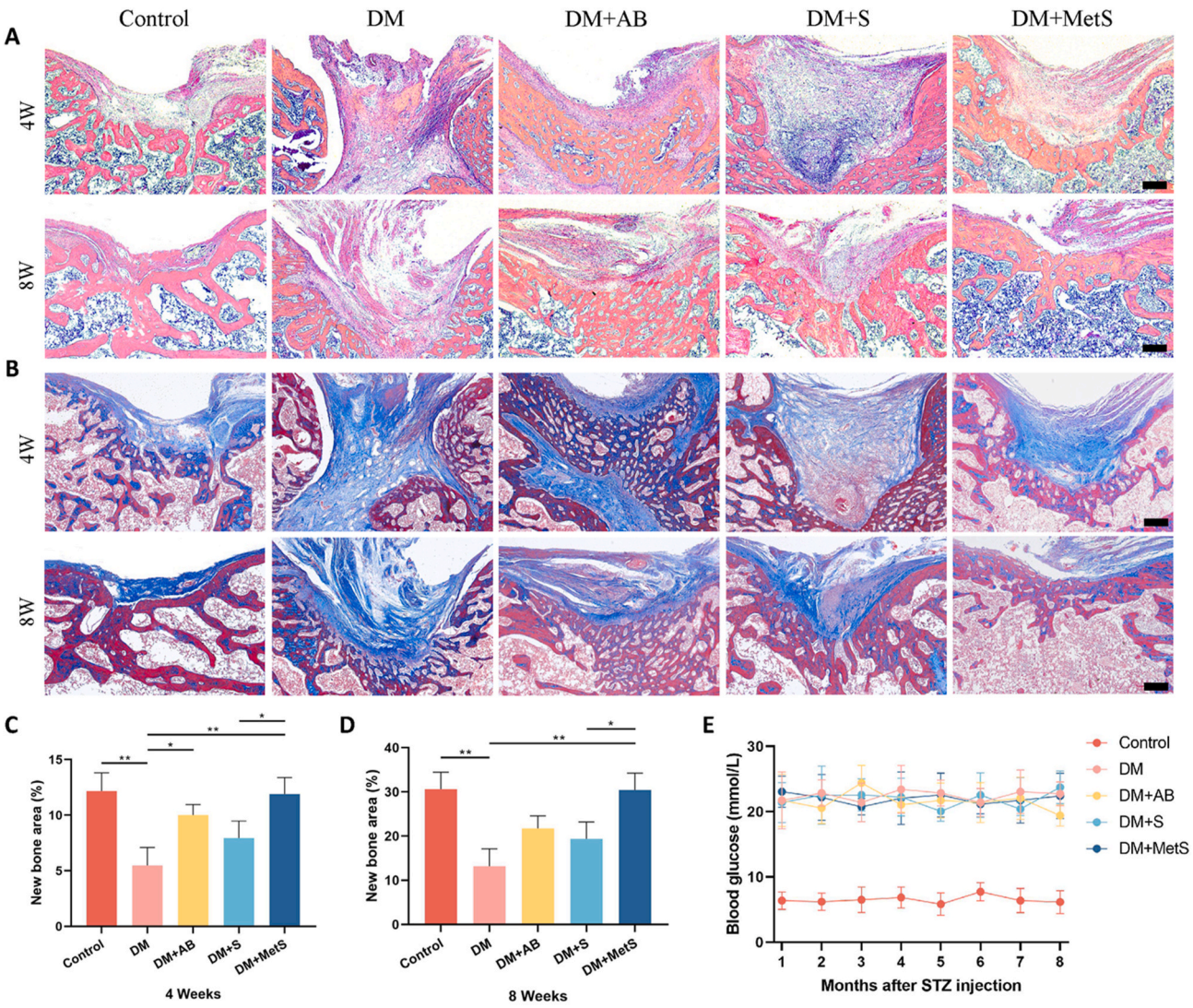

Fig. 5. Representative pictures of A) H&E staining and B) Masson staining of bone tissue sections treated for 4 and 8 weeks in each group (scale bar: 250 μm). New bone area was assessed by bone histomorphometry at C) 4 weeks and D) 8 weeks. E) Blood glucose levels were detected consecutively after STZ injection. (DM: diabetes mellitus, AB: autologous bone, MetS: Metformin scaffolds; n = 6 per group, data are provided as means ± SD, *$p < 0.05$, **$p < 0.01$).

biomaterials known for their exceptional biocompatibility [22]. Notably, Nanoclay possesses inherent osteogenic properties, providing an additional therapeutic advantage to the hydrogel [23].

Previous studies have demonstrated the potential of hybrid bioprinting techniques to enhance the mechanical properties of hydrogels for bone repair [24,25]. In this study, employing a strategy involving the addition of Nanoclay, we successfully printed hydrogel scaffolds with favorable degradation rates, swelling capacities and mechanical strength. Subsequently, three concentrations of metformin were loaded into the GelMA-Nanoclay hydrogel, and the drug release performance was evaluated. As depicted in the results, the release of metformin exhibited a relatively rapid rate within the initial 5 days, followed by a stable release over two months. This favorable release profile highlights the excellent drug delivery capability of the designed metformin-loaded GelMA-Nanoclay hydrogel. Incorporating nanoclay into GelMA hydrogel can alter its degradation rate through various mechanisms, such as enhancing cross-linking density, creating a barrier effect, and increasing the hydrophobicity of GelMA, ultimately achieving the goal of sustained drug release [13,26]. The relationship between metformin and bone regeneration in a high-glucose environment has been widely explored in previous studies. Metformin promotes the differentiation and mineralization of osteoblasts in a high-glucose environment by regulating the RAGE-JAK2-STAT1 signaling axis, significantly improving diabetes-induced osteopenia. Additionally, metformin reverses the adverse effects of high glucose on osteoblasts by activating the adenosine monophosphate-activated protein kinase (AMPK) signaling pathway and upregulating the expression of eNOS and BMP-2, leading to increased gene expression of ALP, Col-I, OCN, and RUNX2 [27,28]. These findings indicate that metformin has potential clinical applications in bone regeneration. Although GelMA, nanoclay, and metformin have each been extensively studied for bone regeneration, our research demonstrates a novel approach by integrating metformin into a 3D printed hydrogel scaffold for localized delivery, showing significant efficacy in enhancing bone regeneration in diabetic bone defects. Furthermore, the hydrogel scaffold used in this study, loaded with 5 mg/mL metformin, releases the drug at a sustained concentration of approximately 1.8 μg/mL. This concentration is close to the plasma concentration of 2 μg/mL observed in patients after oral administration of metformin, thereby aligning closely with clinical conditions [18].

The proliferation and migration of BMSCs play a crucial role in the bone regeneration process [29]. Our investigation revealed that in a high-glucose culture medium, BMSC proliferation and migration were markedly sluggish, and the hydrogel scaffold extract loaded with metformin significantly enhanced the proliferation and migration capacity

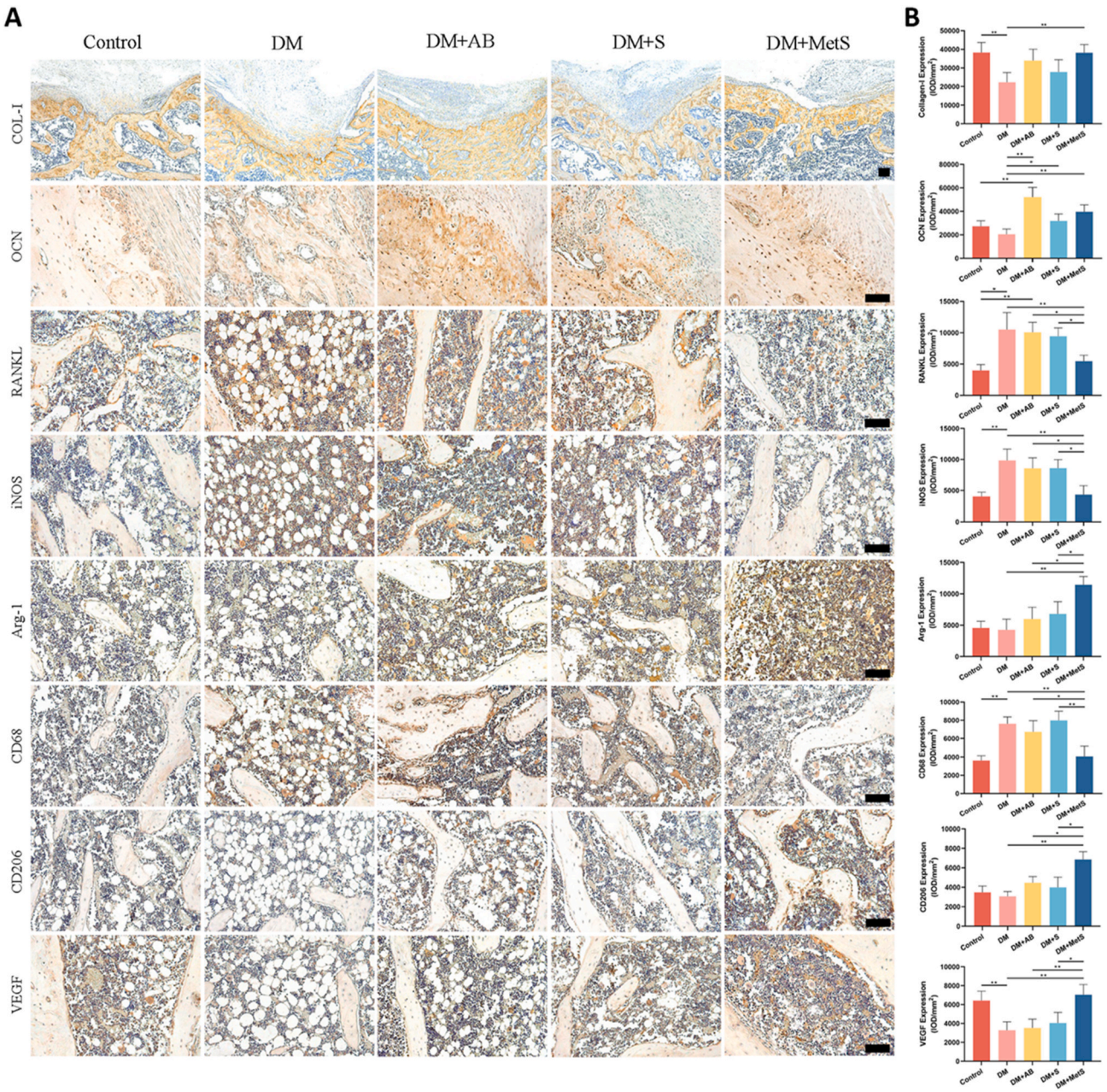

Figure 6. A) Representative immunohistochemical staining of Col-I, OCN, RANKL, iNOS, Arg-1, CD68, CD206 and VEGF in bone defect areas (scale bar: 100 μm). B) Semi-quantification of positively stained in A) (DM: diabetes mellitus, AB: autologous bone, MetS: Metformin scaffolds; n = 6 per group, data are provided as means ± SD, *$p < 0.05$, **$p < 0.01$).

of stem cells in a high-glucose environment. In a study by Zhou et al., an in vitro high-glucose environment was simulated, and metformin intervention was found to significantly improve both cell proliferation and osteogenesis [30]. Culturing BMSCs with extracts from hydrogel scaffolds not loaded with metformin slightly increase ALP activity and calcium nodule density. This outcome may be attributed to the osteogenic effects of magnesium and silicon released from nanoclay. These studies suggest that nanoclay itself has the ability to enhance the osteogenic differentiation of human adipose-derived stem cells (ADSCs) [31]. Nevertheless, the addition of metformin significantly enhanced the osteogenic capability of BMSCs in a high-glucose environment. The potential mechanism lies in metformin's ability to counteract the osteogenic inhibition induced by high glucose. This is achieved through the upregulation of expression of osteogenesis and autophagy-related genes in the high-glucose microenvironment [32]. Furthermore, the results of flow cytometry and qRT-PCR analysis revealed that hydrogel scaffolds loaded with metformin also exhibited outstanding capabilities for angiogenesis and immunomodulation in vitro, and our findings align consistently with these prior studies [33,34]. The aforementioned results suggest that the GelMA-Nanoclay-Metformin hydrogel scaffold not only promotes osteogenesis, angiogenesis and modulates the immune response in a high-glucose microenvironment but also synergistically enhances the interplay among these processes.

Due to the significant differences between in vitro and in vivo microenvironments, we subsequently evaluated the biological functions of the 3D-printed hydrogel scaffolds in vivo. Evidently, micro-CT results showed that the bone volume increased over time in each group, with the DM + MetS group inducing superior bone regeneration in diabetic bone defects compared to the others. This advantage was corroborated by the quantification of BMD, BV/TV and Tb.N. Similar results were also

observed with H&E and Masson staining, along with corresponding histomorphometric analysis. The intrinsic healing process of bone defects is influenced by glucose fluctuations, pro-inflammatory factors, and angiogenesis, leading to inhibited osteogenic activity under diabetic conditions [35]. Despite this, the presence of metformin can activate AMPK, which plays a crucial role in cellular energy homeostasis. This activation leads to enhanced osteoblast differentiation and bone formation. Additionally, metformin upregulates the expression of RUNX2 and Sirt1, which are also critical factors for bone formation and remodeling under diabetic conditions [34,36]. At 8 weeks, trabecular bone structure was gradually remodeled in the Control and DM + MetS groups, while limited remodeling was observed in DM and DM + S groups, indicating suboptimal bone repair. Interestingly, higher bone density and disorganized trabecular bone were also observed in animals with diabetic bone defects undergoing autologous bone transplantation. While autologous bone transplantation remains the optimal treatment for bone defects, in diabetic individuals, reduced blood flow and impaired neovascularization may lead to abnormal bone remodeling, resulting in decreased bone quality and structural disorder of cancellous bone [37,38].

Immunohistochemical staining of COL-I, OCN, and RANKL serves as a reflection of the delicate balance between osteogenesis and osteoclast activity. Autologous bone, scaffolds, and metformin scaffolds each exhibit varying degrees of promotion of OCN expression. Notably, only the hydrogel scaffold loaded with metformin significantly reduces the expression of RANKL. Semi-quantitative analysis reveals that the bone remodeling status at the site of the bone defect in the DM + MetS group closely approximates a normal level. Prior research has established that metformin, by activating AMPK and mTOR, inhibits RANKL-stimulated osteoclast formation and fosters the differentiation of BMSCs into osteoblasts [39]. In addition, the substantial secretion of pro-inflammatory factors by M1 macrophages is a critical challenge in the treatment of diabetic bone defects [40]. Prolonged elevation of inflammatory markers can lead to chronic inflammation, bone loss, and diminished bone mechanical strength, ultimately impeding the healing of bone defects. Numerous studies have demonstrated metformin's selective inhibition of human monocyte differentiation into pro-inflammatory macrophages (M1) without affecting their differentiation into anti-inflammatory macrophages (M2) [41]. Our study consistently reaffirms this property, observing that the in situ release of metformin significantly reduces the macrophage marker CD68 and the M1 macrophage marker iNOS at the site of local diabetic bone defects, while significantly increasing the expression of the M2 macrophage markers Arg-1 and CD206. This suggests that the alleviation of local inflammation may constitute a potential mechanism by which GelMA-Nanoclay-Metformin hydrogel promotes osteogenesis in diabetic bone defects. Furthermore, VEGF immunohistochemical staining indicates an increased angiogenic capacity during bone reconstruction, contributing to the acceleration of bone repair in the diabetic microenvironment. Past studies have demonstrated that metformin, in coordination with mesenchymal cells, can enhance VEGF-mediated angiogenesis in diabetic wound healing, human umbilical cord mesenchymal stem cells treated with metformin exhibit potent efficacy in vitro and in vivo angiogenesis [9,42].

All these findings underscore the potential application of GelMA-Nanoclay-Metformin hydrogel scaffolds in modulating macrophages and alleviating inflammation to enhance bone regeneration and vascularization under high-glucose and chronic inflammatory conditions. Although the defect in DM + MetS group was still not fully bridged and repaired after 2 months of observation, these results still demonstrate that the in situ release of metformin produced by the GelMA-Nanoclay-Metformin hydrogel scaffolds stimulates immunomodulatory functions to coordinate bone regeneration in the diabetic microenvironment. One of the primary limitations of this study is the absence of a comparative analysis between the local delivery of metformin and its systemic administration. Although our results demonstrate the efficacy of local delivery in enhancing osteogenesis, angiogenesis, and immunomodulation in diabetic bone defects, it is crucial to understand how this approach fares against systemic delivery. The mechanical strength of the GelMA-Nanoclay hydrogel scaffold, although optimized, remains relatively low, only achieving a few MPa, which may affect its ability to support weight-bearing applications. Future studies should include a direct comparison of delivery methods, enhance the mechanical properties of scaffold, and elucidate the specific pathways involved in metformin's action on bone tissue under diabetic conditions. By addressing these limitations, the potential of metformin-loaded GelMA-Nanoclay hydrogel scaffolds for treating diabetic bone defects can be better understood and optimized, paving the way for more effective clinical applications.

5. Conclusions

In this study, we introduced an innovative approach by developing a 3D-printed hydrogel scaffold loaded with metformin for the in situ treatment of diabetic bone defects. GelMA creates an environment conducive to cell proliferation and adhesion, while Nanoclay enhances the mechanical strength of the hydrogel and exhibits osteogenic properties. Crucially, metformin improves osteogenesis, angiogenesis, and anti-inflammatory effects under hyperglycemic conditions. In essence, metformin-loaded hydrogel scaffolds can evoke immune regulatory functions, orchestrating diabetic bone regeneration through localized drug release. This novel application of conventional drugs holds promise for consideration in clinical interventions for diabetic bone defects.

Ethics approval and consent to participate

The animal protocol was approved by the Animal Ethics Committee of the Southern Medical University Shenzhen Hospital (NO. 2023-0382).

Consent for publication

Not applicable.

Funding

This research was funded by the Shenzhen Science and Technology Program (JCYJ20200109150641992), Shenzhen Science and Technology Program (JCYJ20210324115814040) and Shenzhen Science and Technology Program (JCYJ20220818103417037).

Declaration of competing interest

Authors are required to disclose commercial or similar relationships to products or companies mentioned in or related to the subject matter of the article being submitted. Affiliations of authors should include corporate appointments relating to or in connection with products or companies mentioned in the article, or otherwise bearing on the subject matter thereof. Sources of funding for the article should be included in the acknowledgments. Other pertinent financial relationships, such as consultancies, stock ownership, or other equity interests or patent-licensing arrangements, should be disclosed in the cover letter to the Editor-in-Chief, on a separate conflict of interest page in the manuscript (see below for examples of how to format the conflict of interest page in your manuscript) and on the conflict of interest form accompanying the article at the time of submission. The conflict of interest form, which is available at:http://www.springer.com/774, should be signed, scanned and submitted through Editorial Manager. The conflicts of interest disclosed on the conflict of interest form should be the same as those disclosed on the conflict of interest page in the manuscript. Questions about this policy should be directed to the Editor-in-Chief.

Acknowledgements

During the preparation of this work the authors used ChatGPT in order to polish some sentences. After using this tool, the authors reviewed and edited the content as needed and take full responsibility for the content of the publication.

Appendix A. Supplementary data

Supplementary data to this article can be found online at https://doi.org/10.1016/j.jot.2024.06.013.

References

[1] Böni-Schnetzler M, Meier DT. Islet inflammation in type 2 diabetes. Semin Immunopathol 2019;41:501–13.
[2] Saeedi P, Petersohn I, Salpea P, Malanda B, Karuranga S, Unwin N, et al. Global and regional diabetes prevalence estimates for 2019 and projections for 2030 and 2045: results from the International Diabetes Federation Diabetes Atlas, 9(th) edition. Diabetes Res Clin Pract 2019;157:107843.
[3] Tao T, Xu H. Autophagy and obesity and diabetes. Adv Exp Med Biol 2020;1207:445–61.
[4] Song F, Lee WD, Marmo T, Ji X, Song C, Liao X, et al. Osteoblast-intrinsic defect in glucose metabolism impairs bone formation in type II diabetic male mice. Elife 2023;12:e85714.
[5] Lee JH, Kong SC, Chen CH, Lin YC, Lee KT, Wang YH. The effects of photobiomodulation on bone defect repairing in a diabetic rat model. Int J Mol Sci 2021;22:119–27.
[6] Lv Z, Guo Y. Metformin and its benefits for various diseases. Front Endocrinol 2020;11:191.
[7] Chen B, He Q, Yang J, Pan Z, Xiao J, Chen W, et al. Metformin suppresses oxidative stress induced by high glucose via activation of the Nrf2/HO-1 signaling pathway in type 2 diabetic osteoporosis. Life Sci 2023;312:121092.
[8] Li D, Ruan G, Zhang Y, Zhao Y, Zhu Z, Ou Q, et al. Metformin attenuates osteoarthritis by targeting chondrocytes, synovial macrophages and adipocytes. Rheumatology 2023;62:1652–61.
[9] Du F, Liu M, Wang J, Hu L, Zeng D, Zhou S, et al. Metformin coordinates with mesenchymal cells to promote VEGF-mediated angiogenesis in diabetic wound healing through Akt/mTOR activation. Metab, Clin Exp 2023;140:155398.
[10] Gao X, Qin W, Chen L, Fan W, Ma T, Schneider A, et al. Effects of targeted delivery of metformin and dental pulp stem cells on osteogenesis via demineralized dentin matrix under high glucose conditions. ACS Biomater Sci Eng 2020;6:2346–56.
[11] Qu L, Dubey N, Ribeiro JS, Bordini EAF, Ferreira JA, Xu J, et al. Metformin-loaded nanospheres-laden photocrosslinkable gelatin hydrogel for bone tissue engineering. J Mech Behav Biomed Mater 2021;116:104293.
[12] Yue K, Trujillo-de Santiago G, Alvarez MM, Tamayol A, Annabi N, Khademhosseini A. Synthesis, properties, and biomedical applications of gelatin methacryloyl (GelMA) hydrogels. Biomaterials 2015;73:254–71.
[13] Jin Y, Liu C, Chai W, Compaan A, Huang Y. Self-supporting nanoclay as internal scaffold material for direct printing of soft hydrogel composite structures in air. ACS Appl Mater Interfaces 2017;9:17456–65.
[14] Ahlfeld T, Cidonio G, Kilian D, Duin S, Akkineni AR, Dawson JI, et al. Development of a clay based bioink for 3D cell printing for skeletal application. Biofabrication 2017;9:034103.
[15] Zhai X, Hou C, Pan H, Lu WW, Liu W, Ruan C. Nanoclay incorporated polyethylene-glycol nanocomposite hydrogels for stimulating in vitro and in vivo osteogenesis. J Biomed Nanotechnol 2018;14:662–74.
[16] Gao F, Zhang Y, Li Y, Xu B, Cao Z, Liu W. Sea cucumber-inspired autolytic hydrogels exhibiting tunable high mechanical performances, repairability, and reusability. ACS Appl Mater Interfaces 2016;8:8956–66.
[17] Wu Z, Bai J, Ge G, Wang T, Feng S, Ma Q, et al. Regulating macrophage polarization in high glucose microenvironment using lithium-modified bioglass-hydrogel for diabetic bone regeneration. Adv Healthcare Mater 2022;11:e2200298.
[18] Sutkowska E, Fortuna P, Wisniewski J, Sutkowska K, Hodurek P, Gamian A, et al. Low metformin dose and its therapeutic serum concentration in prediabetes. Sci Rep 2021;11:11684.
[19] Tian P, Zhao L, Kim J, Li X, Liu C, Cui X, et al. Dual stimulus responsive borosilicate glass (BSG) scaffolds promote diabetic alveolar bone defectsrepair by modulating macrophage phenotype. Bioact Mater 2023;26:231–48.
[20] Camacho-Alonso F, Tudela-Mulero MR, Buendía AJ, Navarro JA, Pérez-Sayáns M, Mercado-Díaz AM. Bone regeneration in critical-sized mandibular symphysis defects using bioceramics with or without bone marrow mesenchymal stem cells in healthy, diabetic, osteoporotic, and diabetic-osteoporotic rats. Dent Mater : official publication of the Academy of Dental Materials 2022;38:1283–300.
[21] Luo M, Zhao Z, Yi J. Osteogenesis of bone marrow mesenchymal stem cell in hyperglycemia. Front Endocrinol 2023;14:1150068.
[22] Zhou B, Jiang X, Zhou X, Tan W, Luo H, Lei S, et al. GelMA-based bioactive hydrogel scaffolds with multiple bone defect repair functions: therapeutic strategies and recent advances. Biomater Res 2023;27:86.
[23] Zhang YD, Ma AB, Sun L, Chen JD, Hong G, Wu HK. Nanoclay-modified hyaluronic acid microspheres for bone induction by sustained rhBMP-2 delivery. Macromol Biosci 2023;24:e2300245.
[24] Kim BS, Jang J, Chae S, Gao G, Kong JS, Ahn M, et al. Three-dimensional bioprinting of cell-laden constructs with polycaprolactone protective layers for using various thermoplastic polymers. Biofabrication 2016;8:035013.
[25] Lai J, Wang C, Liu J, Chen S, Liu C, Huang X, et al. Low temperature hybrid 3D printing of hierarchically porous bone tissue engineering scaffolds within situdelivery of osteogenic peptide and mesenchymal stem cells. Biofabrication 2022;14:108–14.
[26] Aldana AA, Malatto L, Rehman MAU, Boccaccini AR, Abraham GA. Fabrication of gelatin methacrylate (GelMA) scaffolds with nano- and micro-topographical and morphological features. Nanomaterials 2019;9:14–21.
[27] Lin R, Xu B, Ye Z, Gao Y, Fang H, Song J, et al. Metformin attenuates diabetes-induced osteopenia in rats is associated with down-regulation of the RAGE-JAK2-STAT1 signal axis. Journal of orthopaedic translation 2023;40:37–48.
[28] Zhu Z, Gao S, Zhu H, Chen Y, Wu D, Chen Z, et al. Metformin improves fibroblast metabolism and ameliorates arthrofibrosis in rats. Journal of orthopaedic translation 2023;40:92–103.
[29] Qin Q, Lee S, Patel N, Walden K, Gomez-Salazar M, Levi B, et al. Neurovascular coupling in bone regeneration. Exp Mol Med 2022;54:1844–9.
[30] Zhou X, Kuang Y, Liang S, Wang L. Metformin inhibits cell proliferation in SKM-1 cells via AMPK-mediated cell cycle arrest. J Pharmacol Sci 2019;141:146–52.
[31] Zheng X, Zhang X, Wang Y, Liu Y, Pan Y, Li Y, et al. Hypoxia-mimicking 3D bioglass-nanoclay scaffolds promote endogenous bone regeneration. Bioact Mater 2021;6:3485–95.
[32] Zhou R, Ma Y, Qiu S, Gong Z, Zhou X. Metformin promotes cell proliferation and osteogenesis under high glucose condition by regulating the ROS-AKT-mTOR axis. Mol Med Rep 2020;22:3387–95.
[33] Gu Q, Gu Y, Yang H, Shi Q. Metformin enhances osteogenesis and suppresses adipogenesis of human chorionic villous mesenchymal stem cells. Tohoku J Exp Med 2017;241:13–9.
[34] Mu W, Liang G, Feng Y, Jiang Y, Qu F. The potential therapeutic role of metformin in diabetic and non-diabetic bone impairment. Pharmaceuticals 2022;15:123–34.
[35] Li D, Chen K, Tang H, Hu S, Xin L, Jing X, et al. A logic-based diagnostic and therapeutic hydrogel with multistimuli responsiveness to orchestrate diabetic bone regeneration. Adv Mater 2022;34:e2108430.
[36] Guo Y, Wei J, Liu C, Li X, Yan W. Metformin regulates bone marrow stromal cells to accelerate bone healing in diabetic mice. Elife 2023;12:101231.
[37] Lecka-Czernik B. Diabetes, bone and glucose-lowering agents: basic biology. Diabetologia 2017;60:1163–9.
[38] Gillman CE, Jayasuriya AC. FDA-approved bone grafts and bone graft substitute devices in bone regeneration. Mater Sci Eng C 2021;130:112466.
[39] Kim YS, Park BS, Baek HS, Kang HM, Oh JM, Kim IR. Metformin activates AMPK and mTOR to Inhibit RANKL-stimulated osteoclast formation. Eur Rev Med Pharmacol Sci 2023;27:8795–811.
[40] Sun X, Ma Z, Zhao X, Jin W, Zhang C, Ma J, et al. Three-dimensional bioprinting of multicell-laden scaffolds containing bone morphogenic protein-4 for promoting M2 macrophage polarization and accelerating bone defect repair in diabetes mellitus. Bioact Mater 2021;6:757–69.
[41] Nassif RM, Chalhoub E, Chedid P, Hurtado-Nedelec M, Raya E, Dang PM, et al. Metformin inhibits ROS production by human M2 macrophages via the activation of AMPK. Biomedicines 2022;10:234–41.
[42] Lei T, Deng S, Chen P, Xiao Z, Cai S, Hang Z, et al. Metformin enhances the osteogenesis and angiogenesis of human umbilical cord mesenchymal stem cells for tissue regeneration engineering. Int J Biochem Cell Biol 2021;141:106086.